

RESEARCH

Open Access



Increased extracellular fluid is associated with white matter fiber degeneration in CADASIL: in vivo evidence from diffusion magnetic resonance imaging

Xinfeng Yu^{1†}, Xinzhen Yin^{2†}, Hui Hong¹, Shuyue Wang¹, Yeerfan Jiaerken¹, Fan Zhang³, Ofer Pasternak^{3,4}, Ruiting Zhang¹, Linglin Yang⁵, Min Lou², Minming Zhang^{1*} and Peiyu Huang^{1*} 

Abstract

Background: White matter hyperintensities (WMHs) are one of the hallmarks of cerebral small vessel disease (CSVD), but the pathological mechanisms underlying WMHs remain unclear. Recent studies suggest that extracellular fluid (ECF) is increased in brain regions with WMHs. It has been hypothesized that ECF accumulation may have detrimental effects on white matter microstructure. To test this hypothesis, we used cerebral autosomal-dominant arteriopathy with subcortical infarcts and leukoencephalopathy (CADASIL) as a unique CSVD model to investigate the relationships between ECF and fiber microstructural changes in WMHs.

Methods: Thirty-eight CADASIL patients underwent 3.0 T MRI with multi-model sequences. Parameters of free water (FW) and apparent fiber density (AFD) obtained from diffusion-weighted imaging ($b = 0$ and 1000 s/mm^2) were respectively used to quantify the ECF and fiber density. WMHs were split into four subregions with four levels of FW using quartiles (FWq1 to FWq4) for each participant. We analyzed the relationships between FW and AFD in each subregion of WMHs. Additionally, we tested whether FW of WMHs were associated with other accompanied CSVD imaging markers including lacunes and microbleeds.

Results: We found an inverse correlation between FW and AFD in WMHs. Subregions of WMHs with high-level of FW (FWq3 and FWq4) were accompanied with decreased AFD and with changes in FW-corrected diffusion tensor imaging parameters. Furthermore, FW was also independently associated with lacunes and microbleeds.

Conclusions: Our study demonstrated that increased ECF was associated with WM degeneration and the occurrence of lacunes and microbleeds, providing important new insights into the role of ECF in CADASIL pathology. Improving ECF drainage might become a therapeutic strategy in future.

Keywords: White matter, Extracellular fluid, Cerebral small vessel diseases, CADASIL, MRI, Diffusion-weighted imaging

Introduction

White matter hyperintensities (WMHs) on MRI scans are one of the hallmarks of cerebral small vessel disease (CSVD), which are associated with cognitive impairment, dementia, stroke and even death [1–3]. However, the pathological mechanisms leading to WMHs remain unclear. WMHs are the earliest and most frequent

*Correspondence: huangpy@zju.edu.cn; zhangminming@zju.edu.cn;

huangpy@zju.edu.cn; zhangminming@zju.edu.cn

[†]Xinfeng Yu and Xinzhen Yin contributed equally

¹ Department of Radiology, The 2nd Affiliated Hospital, Zhejiang University School of Medicine, No.88 Jiefang Road, Shangcheng District, Hangzhou 310009, China

Full list of author information is available at the end of the article



observed imaging feature in cerebral autosomal-dominant arteriopathy with subcortical infarcts and leukoencephalopathy (CADASIL) [4] which is a monogenic CSVD caused by Notch 3 gene mutations [5]. Unlike sporadic CSVD, the occurrence and progression of WMHs are less dependent on cardiovascular risk factors and age in CADASIL [6]. Therefore, CADASIL could serve as a unique model for investigating the pathological mechanisms of WMHs.

Accumulating studies of CADASIL provide the evidence that WMHs are strongly related to increased extracellular fluid (ECF). For example, a neuropathological study has demonstrated that WMHs in the anterior temporal lobe of CADASIL reflect fluid accumulation in enlarged perivascular spaces (PVS), together with the loss of WM [7]. A recent study of CADASIL patients reveals that changes in diffusion MRI signals within WMHs are mainly driven by increased extracellular free water [8]. Furthermore, ECF are differentially distributed in the WMHs, with higher ECF in specific regions of WMHs such as anterior temporal lobe [9]. However, the association between increased ECF and white matter (WM) microstructural changes in WMHs has not yet been determined. It has been argued that increased ECF would result in a build-up of substances toxic (e.g., plasma proteins) to the WM microstructure [10, 11]. Although diffusion tensor imaging (DTI) is a well-established method for quantifying microstructural WM alterations in vivo, the model fitting would be largely influenced by the extracellular water and intravoxel crossing fibers which happen to be seen in WMHs [12].

Recent diffusion MRI methods applying novel post-processing approaches can be used to achieve more direct in vivo characterization of both intra- and extracellular properties of WM tissue. For example, free water (FW) imaging using bi-tensor model could potentially separate the diffusion signals from extracellular FW and tissue compartment [13]. Apparent fiber density (AFD) imaging using constrained spherical deconvolution (CSD) allows the resolution of crossing fibers in voxels containing multiple fiber orientations, and it could estimate the fraction of space occupied by a fiber bundle [14].

In this study, in a cohort of patients with CADASIL, we characterized the ECF (indexed by FW) and fiber density (indexed by AFD) in WMHs using the two advanced diffusion approaches. We hypothesized that increased ECF would be associated with fiber microstructural changes in WMHs. Considering the heterogeneity of ECF distribution in WMHs, we classified FW in individual WMHs into four levels using quartiles and used lesion probability map (LPM) to understand the distribution of different levels of ECF in WMHs. We analyzed the relationships between different levels of ECF and microstructural

diffusion metrics (including AFD and FW-corrected DTI metrics). Given that WMHs commonly accompany lacunes and microbleeds, we further explored the correlations between ECF in WMHs with both lacunes and microbleeds.

Methods

Participants

The study was approved by the Medical Ethics Committee of the Second Affiliated Hospital, Zhejiang University School of Medicine and written informed consent was obtained from all subjects. We enrolled 38 patients with CADASIL. The diagnosis of CADASIL was confirmed by genetic testing with a pathogenic mutation in the Notch 3 gene which has been described in our previous study [15]. The following clinical variables were documented for each subject: age, gender, the history of hypertension, diabetes mellitus, hyperlipidemia, and smoking. In addition, the presence/absence of symptoms including transient ischemic attack/stroke, headache, psychiatric and cognitive impairments were also recorded. The disease duration was defined as the length of time between initial symptom onset and brain MRI examination.

Data acquisition

All patients were examined using a 3.0 T whole body-scanner (Discovery MR750, GE Healthcare, Milwaukee, WI) equipped with an 8-channel phased array head coil. The details of MR sequence are shown in Additional file 1: Methods.

Image processing

Overview of the image processing pipeline for each subject is shown in Fig. 1.

Diffusion preprocessing

The preprocessing steps of diffusion data included denoising, eddy-current and echo-planar imaging (EPI) distortion correction and motion correction, gibbs ringing removal, bias-field correction. In addition to EPI distortion, the preprocessing steps were processed using a combination of commands in the MRtrix3 package, FMRIB Software Library (FSL) and Advanced Normalization Tools (ANTs). The EPI distortion was corrected using the bdp correction algorithm implemented in the BrainSuite software package (<https://brainsuite.org>).

Free water estimation

FW analysis has been described in detail elsewhere [8, 13, 16]. Briefly, the preprocessed diffusion data was fitted with a bi-tensor model within each voxel: the first one models FW diffusion, defining as an isotropic diffusion, and the second one models the tissue compartment. The

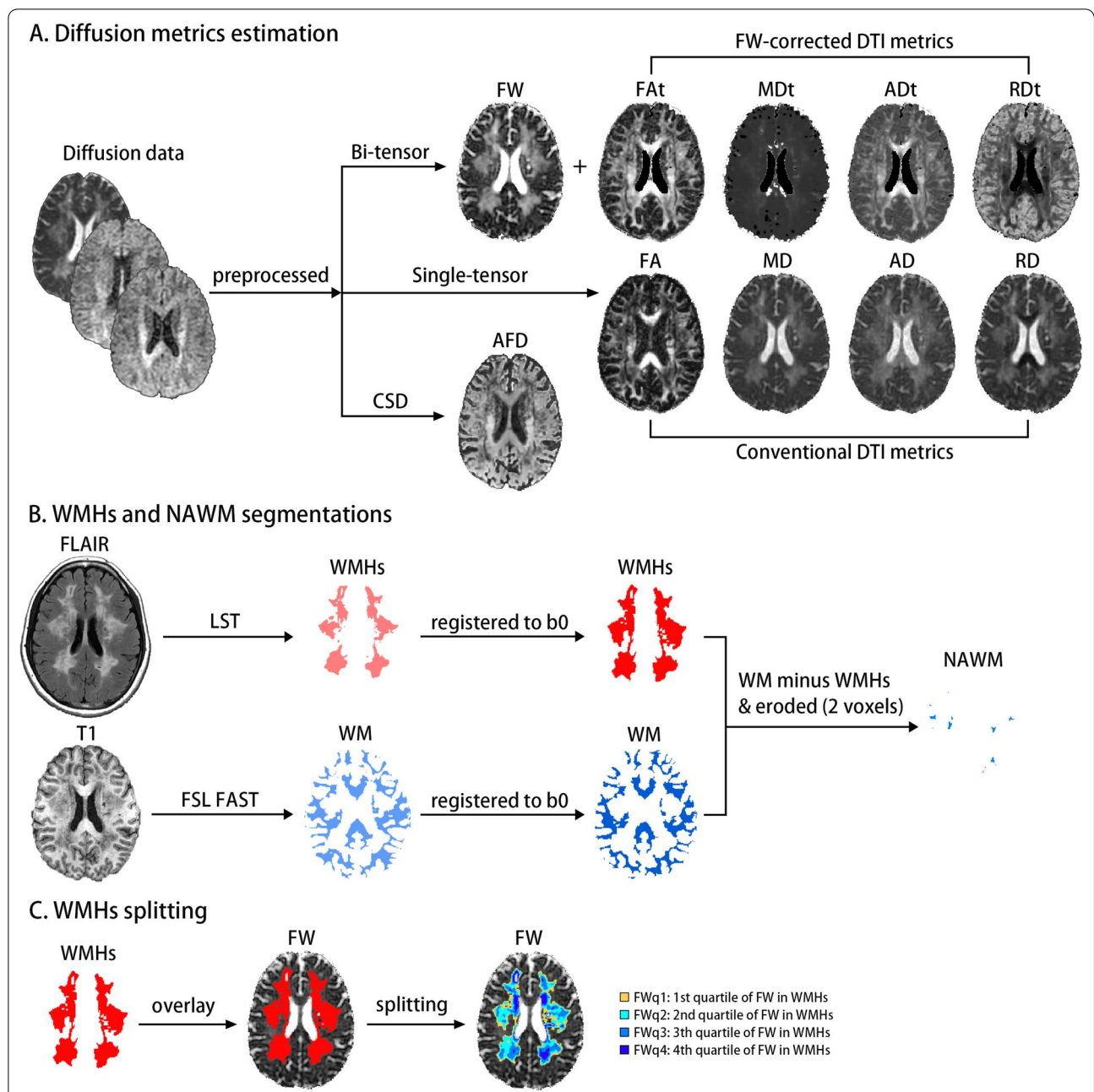


Fig. 1 Overview of the image processing pipeline for each subject. **A** The single-shell diffusion data ($b=0, 1000 \text{ s/mm}^2$) were preprocessed and then were separately fitted into bi-tensor, single tensor and CSD models. The diffusion parameters including FW, FW-corrected DTI metrics (FAt, MDt, ADt, RDt) and conventional DTI metrics (FA, MD, AD, RD) were estimated. **B** WMHs mask was created by FLAIR image using the toolbox of LST in SPM12 and WM mask was generated from T1 image using FSL FAST. Both masks of WMHs and WM were co-registered into the individual $b=0 \text{ s/mm}^2$ (b_0) image using ANTs. Then, NAWM was made by subtracting the WMHs mask from the WM mask, and it was subsequently eroded by two voxels to avoid partial volume effects. **C** The mask of WMHs was split into four sub-masks with using FW quartiles. CSD constrained spherical deconvolution, FW free water; DTI diffusion tensor imaging, FAt tissue compartment FA, MDt tissue compartment MD; ADt tissue compartment AD, RDt tissue compartment RD, FA fractional anisotropy, MD mean diffusivity, AD axial diffusivity; RD radial diffusivity, AFD apparent fiber density; WMHs white matter hyperintensities, FLAIR T2 flu-id-attenuated inversion recovery; LST = Lesion Segmentation Toolbox; SPM Statistical Parametric Mapping, WM white matter, FSL FMRIB Software Library, FAST FMRIB's Automated Segmentation Tool, ANTs Advanced Normalization Tools, NAWM normal appearing white matter

isotropic compartment models extracellular FW which is characterized by freely and not hindered or restricted diffusion. The fraction of FW content per voxel provided a native FW map and varied between 0 and 1. FW-corrected DTI parameters were further calculated from the tissue compartment's tensor, namely fractional anisotropy (FA), mean diffusivity (MD), axial diffusivity (AD) and radial diffusivity (RD). Besides, the conventional DTI parameters including FA, MD, AD and RD were estimated from the preprocessed diffusion data using linear least squares method [13]. Both FW-corrected and conventional DTI parameters were computed using Matlab R2018b (MathWorks, Natick, MA).

Apparent fiber density estimation

The preprocessed diffusion data were up-sampled, resulting in 1 mm^3 isotropic voxels. Subsequently, the 3-tissue response functions including WM, gray matter (GM), and cerebrospinal fluid (CSF) were directly estimated from the diffusion data themselves for each subject using a robust and fully automated unsupervised method [17]. Then, the response functions obtained from all subjects for each tissue type were averaged. The WM fiber orientation distributions (FODs) for each participant were computed using the group averaged response function via single-shell 3-tissue CSD (SS3T-CSD) in MRtrix3Tissue [18]. Next, the WM FODs were further performed by bias fields correction and global intensity normalization [19]. Finally, the voxel-based AFD map was obtained from the integral of WM FODs [14].

Segmentations of WMHs and NAWM

WMHs were segmented using the FLAIR image by the lesion prediction algorithm implemented in the Lesion Segmentation Toolbox version 3.0.0 (www.statistical-modelling.de/lst.html) in Statistical Parametric Mapping Version 12. This algorithm consists of a binary classifier in the form of a logistic regression model trained on the data of 53 multiple sclerosis patients with severe lesion patterns [20]. Next, we used a threshold of 0.5 to obtain the binary mask for WMHs [21]. The mask of WMHs for each subject was visually checked and further manually corrected for false positives and negatives by an experienced neuroradiologist (X.F.Y) using ITK-SNAP software (www.itksnap.org). Then, WMHs mask was co-registered with the $b=0 \text{ s/mm}^2$ (b_0) image using the transformation matrix of registration from FLAIR image to b_0 image with default parameters using ANTs. The final mask of WMHs (b_0 space) was further checked by the same neuroradiologist (X.F.Y).

WM mask was created by the skull-stripped T1 image using FMRIB's Automated Segmentation Tool. Then, WM mask was co-registered with the b_0 image using the

transformation matrix of registration from T1 image to b_0 image with default parameters using ANTs. Normal appearing white matter (NAWM) mask for each subject was created by subtracting the mask of WMHs from the mask of WM (both masks at the b_0 space), and it was subsequently eroded by two voxels in three dimensions to ensure voxels within the final NAWM mask were not contaminated by partial volume effects. The neuroradiologist (X.F.Y) visually checked the NAWM mask to manually exclude the undesired voxels such as those from WMHs, lacunes, microbleeds and CSF.

To classify extracellular FW at different levels in WMHs, each subject's WMHs mask was split into four sub-masks (FWq1 to FWq4) using FW quartile values within their own WMHs. FWq1 represents the subregions containing lowest 25% of FW values in WMHs, while FWq4 represents the subregions containing highest 25% of FW values in WMHs.

At last, the mean values of diffusion metrics for each subject were extracted from individual masks of WMHs, NAWM as well as each sub-mask of WMHs.

Creating lesion probability map for FW

LPM was used to assess the spatial distribution of FW at each level as previously described [22, 23]. Firstly, T1 images (b_0 space) were normalized to the Montreal Neurological Institute (MNI152) standard space (1 mm^3), and the corresponding matrices were applied to each sub-mask of WMHs with nearest-neighbor interpolation using ANTs. All registrations were checked visually to exclude alignment failures. Then, LPM for each level of FW was generated by averaging the corresponding sub-mask of WMHs using `fslmaths` tool (part of FSL). For each LPM, the resulting voxel intensity indicates how frequently the voxel in question is within a lesion across all patients (i.e., the probability of that voxel being lesional).

Estimation of intracranial volume

Intracranial volumes (ICV) were estimated using T1 image by automatic image processing pipeline of FreeSurfer version 6.0 (<https://surfer.nmr.mgh.harvard.edu>). The total WMHs volume and four subregions of WMHs volumes were all corrected by ICV.

Evaluations of lacunes and microbleeds

The presence of lacunes and microbleeds were evaluated by two radiologists (Y.X.F and H.H). Lacunes were defined as 3- to 15-mm cavitated lesions (CSF-like signals on T1 and FLAIR images) of presumed ischemic origin and distinct from dilated perivascular spaces [24]. Microbleeds were defined as small (diameter $\leq 10 \text{ mm}$) and rounded hypointense lesions on SWI images and microbleeds mimics, such as vessels, calcification, partial

volumes and air/bone interfaces were carefully excluded [24]. The inter-rater agreements for the presence of lacunes and microbleeds between two raters were determined by the Cohen's kappa.

Statistics

Comparisons of diffusion metrics between WMHs and NAWM were performed by paired-t test, and among the four WMHs subregions were analyzed using one-way multivariate analysis of variance (MANOVA) which were followed by post hoc tests with Bonferroni correction. The effect sizes were estimated using generalized eta squared (η^2 [g]). Because the conventional DTI metrics were contaminated by FW, we did not include them in the correlation analysis. We performed the correlations between FW, AFD with FW-corrected DTI metrics using Pearson's correlation. The correlations were further analyzed using partial correlation, after adjusting age, gender and corrected WMHs volume. The correlation coefficients were considered significant at $p < 0.05$ following Bonferroni adjustment for multiple comparisons. We additionally analyzed the relationships between duration of disease with FW and AFD using partial correlation, after adjusting age, gender and corrected WMH volumes. We used logistics regression model to identify the relationships between FW with lacunes and microbleeds. The odds ratio (OR) and its 95% confidence intervals (CI) were estimated. Change-in-estimate approach was used to select variables in a stepwise fashion according to the magnitude of the differences between adjusted and unadjusted effect estimates [25]. A change in the estimated measure of association of 10% or more would be evidence that confounding was present [26]. All statistical analyses were performed in R (version 4.0.3) and SPSS (version 26.0).

Results

Table 1 summarizes the demographic, clinical characteristics and neuroimaging features of CADASIL patients.

Abnormal diffusion metrics in WMHs

Compared with NAWM, FW increased and AFD decreased in WMHs. FAt and ADt were lower in WMHs than in NAWM, while MDt and RDt was higher. For conventional DTI metrics, we found the similar changes in FA, MD and RD, except in AD which showed a change in the opposite direction. The results are shown in Fig. 2.

Correlations between diffusion metrics in WMHs

FW was only significantly correlated with AFD and MDt, and AFD was significantly correlated with FAt, ADt and RDt (Fig. 3). The correlations were slightly stronger after

Table 1 Demographic, clinical, and neuroimaging characteristics of CADASIL patients

	CADASIL (n = 38)
Age, mean (SD), y	49.7 (6.5)
Gender (female), n (%)	27 (71.1)
Duration of disease, median (IQR), y	2 (0.8—5)
Hypertension, n (%)	6 (15.8)
Diabetes mellitus, n (%)	3 (7.9)
Hyperlipidemia, n (%)	3 (7.9)
Smoking, n (%)	3 (7.9)
TIA/Stroke, n (%)	18 (47.4)
Headache, n (%)	22 (57.9)
Cognitive impairment, n (%)	14 (36.8)
Psychiatric impairment, n (%)	17 (44.7)
WMHs volume, mean (SD), ml	81.1 (40.0)
Corrected WMHs volume by ICV, mean (SD)	0.057 (0.027)
With lacunes, n (%)	27 (71.1)
With microbleeds, n (%)	21 (55.3)

CADASIL Cerebral autosomal dominant arteriopathy with subcortical infarcts and leukoencephalopathy, SD standard deviation, IQR interquartile range, TIA transient ischemic attack, WMHs white matter hyperintensities, ICV intracranial volumes

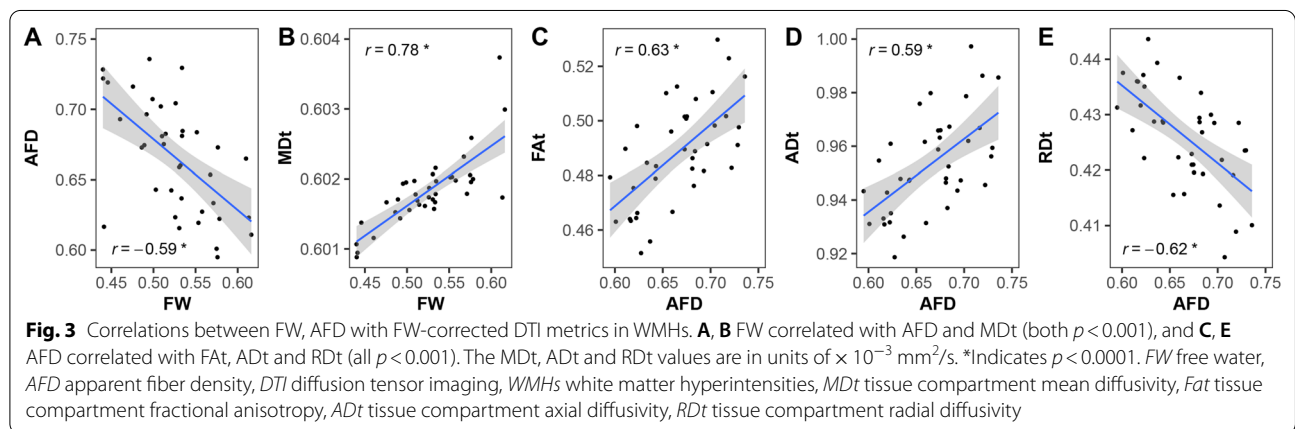
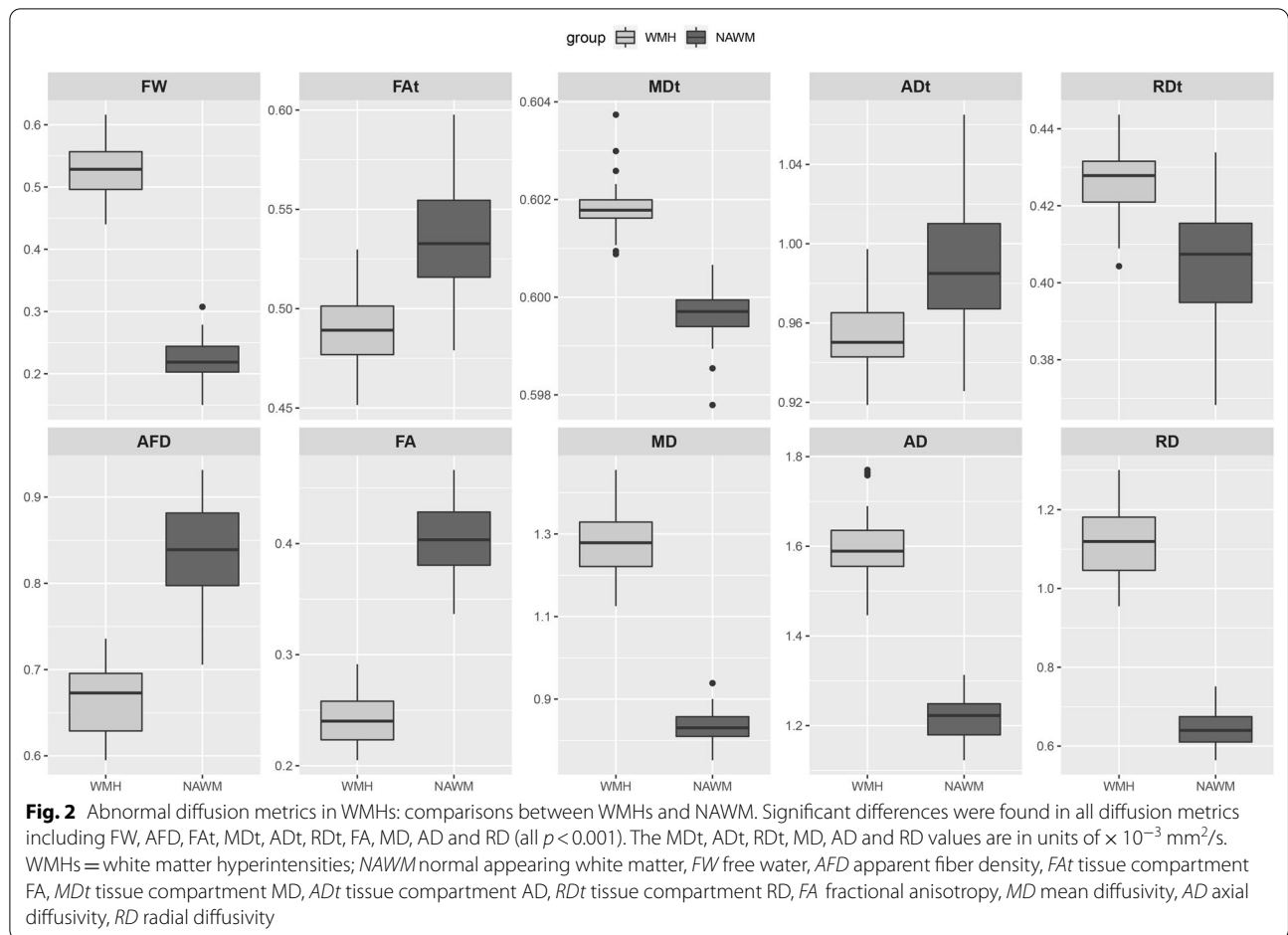
adjusting age, gender and corrected WMHs volumes (Additional file 1: Table S1).

Lesion probability maps for different levels of FW

Figure 4 displays LPMs for FWq1 to FWq4. The lesion distribution of FWq1 appeared to demonstrate a diffusely distributed pattern, mainly in the deep WM. With the increased FW, the more frequent involvement of areas tended to move towards the lateral ventricle (i.e., periventricular predilection). Involvement of anterior temporal lobe was also more frequently seen in subregions with high-level FW (FWq3 and FWq4).

Abnormal diffusion metrics in subregions with different levels of FW

Figure 5 shows comparisons of all diffusion metrics among the four subregions of WMHs. Because each diffusion metric was significantly higher or lower in FWq1 than those in NAWM (Additional file 1: Figure S1), NAWM was not included in the MANOVA analysis. From FWq1 to FWq4, a decreasing gradient was found in AFD ($F = 120.46$, η^2 [g] = 0.71), FAt ($F = 37.80$, η^2 [g] = 0.43) and ADt ($F = 26.29$, η^2 [g] = 0.35) and an increasing gradient was found in MDt ($F = 49.30$, η^2 [g] = 0.50) and RDt ($F = 34.16$, η^2 [g] = 0.41). The similar gradient changes were found in FA ($F = 316.63$, η^2 [g] = 0.87), MD ($F = 374.16$, η^2 [g] = 0.88) and RD ($F = 382.27$, η^2 [g] = 0.89), while an opposite change was found in AD ($F = 306.86$, η^2 [g] = 0.86).



Correlations between diffusion metrics in subregions with different levels of FW

Increased FW was correlated with a decreased AFD in FWq3 and FWq4, and correlated with a higher MDt in FWq1, FWq2 and FWq3. Decreased AFD was correlated with a lower Fat, ADt and a higher RDt in each

subregion of WMHs, and the correlation coefficient becomes stronger with the increased level of FW. The scatter plots of the correlations in each subregion of WMHs are shown in Fig. 6. After adjusting age, gender and corrected WMHs volumes, all the significant correlations were slightly improved (Additional file 1: Table S2).

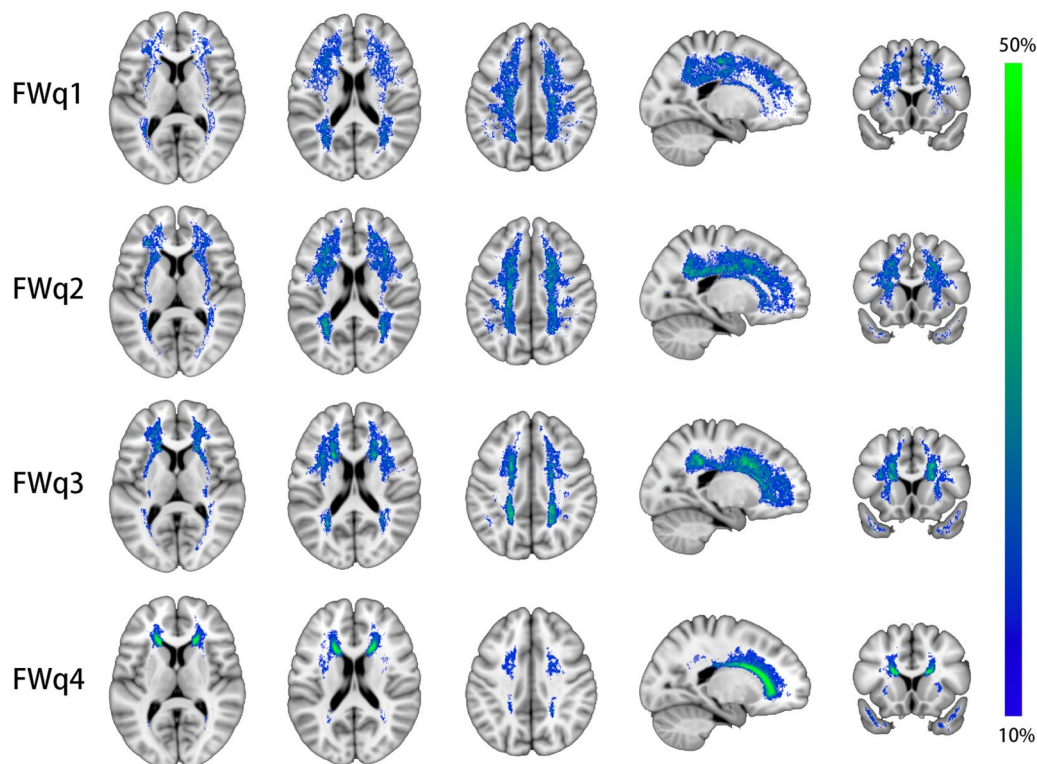


Fig. 4 Distribution pattern of FW in four subregions of WMHs (FWq1-4). The highest frequency of lesion voxels was identified in the anterior horn of the lateral ventricle in FWq4 (peak probability = 0.55, voxel size = 182 mm³). FW free water, WMHs white matter hyperintensities, FWq1-4 four subregions of WMHs split by FW quartiles

Relationships with duration of disease

No significant correlations were found between disease duration with FW and AFD in WMHs ($r=0.137$, $p=0.431$ and $r=-0.271$, $p=0.115$). In four subregions of WMHs, only marginal correlations were found between AFD and duration of disease in FWq3 and FWq4 ($r=-0.305$, $p=0.075$ and $r=-0.285$, $p=0.097$).

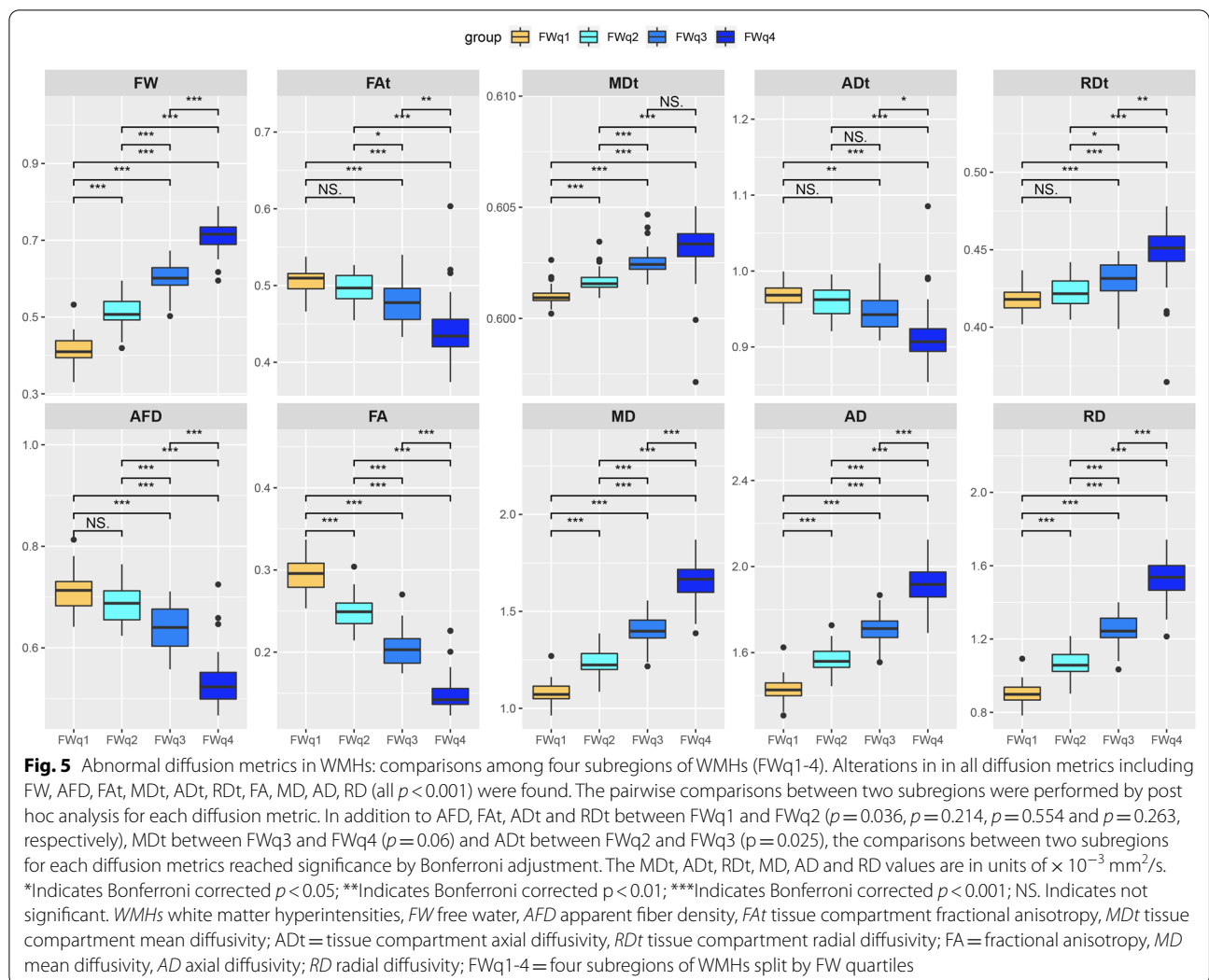
Relationships with lacunes and microbleeds

The interrater agreements for evaluating the presence of lacunes and CMBs were excellent ($\kappa=0.87$, 95% CI = 0.69–1.0; $\kappa=0.95$, 95% CI = 0.85–1.0; respectively). Table 2 showed the relationships between FW with lacunes and microbleeds. The changes in effect estimates after each variable added to the models are shown in Fig. 7. Increased FW independently correlated with the presence of lacunes (OR = 1.33, 95% CI = 1.10–1.71, $p=0.01$). Increased FW also independently correlated with the presence of microbleeds (OR = 1.27, 95% CI = 1.08–1.58, $p=0.01$ and OR = 1.41, 95% CI = 1.15–1.88, $p=0.005$ after adjusting the confounder of hypertension).

Discussion

This study applied two advanced diffusion imaging methods to obtain deeper insight into the pathologic underpinnings of WMHs in CADASIL. In line with our hypothesis, we found an association between increased level of ECF and fiber microstructural changes in WMHs. Furthermore, we found that ECF was independently associated with both lacunes and microbleeds.

The etiology of WMHs involves complex mechanisms such as ischemia [27], blood–brain barrier (BBB) leakage [28], venous collagenosis [29] and impaired perivascular drainage [11]. Most of these mechanisms could lead to interstitial fluid (ISF) accumulation in extracellular spaces and the role of ECF in WMHs has been consistently reported in recent studies. For example, increased aortic stiffness could promote an increase in extracellular water content in WM, eventually leading to the development of WMHs [30]. While the strong relationship between collagenosis of the deep medullary veins and periventricular WMHs has been confirmed in radiological-pathological correlation studies [29, 31, 32], our recent study further suggests that their association is mediated by increased ECF [33]. Moreover, enlarged PVS is hypothesized to represent impaired drainage of ISF from the brain [34]



and the fact that WMHs may grow from dilated PVS also suggests significant contribution of ECF accumulation [35].

To understand the distribution of different levels of ECF within WMHs in our cohort of CADASIL patients, we classified WMHs into four subregions based on the quartiles of FW and mapped the lesion probability of WMHs at each voxel for each quartile of FW. We found that the distribution of ECF in WMHs varied with its levels. Low-level ECF locates mainly at the deep WMHs in frontal and parietal lobes with a diffusely distributed pattern, whereas high-level ECF preferred to locate at the periventricular WMHs. Traditionally, the regional localization of WMHs such as periventricular and deep WMHs would be influenced by different features of vascular anatomy [36]. However, this theory seems difficult to explain the regional localization of ECF because a high level of ECF is also found in the deep WMHs of temporal lobe (i.e., anterior temporal lobe) which is a characteristic

region in CADASIL. Our finding of increased ECF in WMHs of the anterior temporal lobe is consistent with a previous neuropathological study showing that increased ECF is related with enlarged PVS [7] which is an imaging marker of impaired ISF drainage [34]. Therefore, it can be speculated that regional variation of increased ECF in WMHs may reflect the degree of reduced capacity for ISF drainage from the WM.

Under normal conditions, the drainage of ISF and soluble metabolites from brain tissues by the perivascular pathways is necessary to maintain homeostasis in the brain [37]. A pathological hallmark of CADASIL is the early depositions of granular osmiophilic material (GOM) adjacent to basement membranes of arteries, arterioles, and capillaries [38]. It has been suggested that GOM plays a key role in hindering perivascular drainage [38]. Furthermore, the degeneration of vascular smooth muscle cells (VSMCs) in CADASIL reduces vascular tone and amplitude of pulsations for the propagation

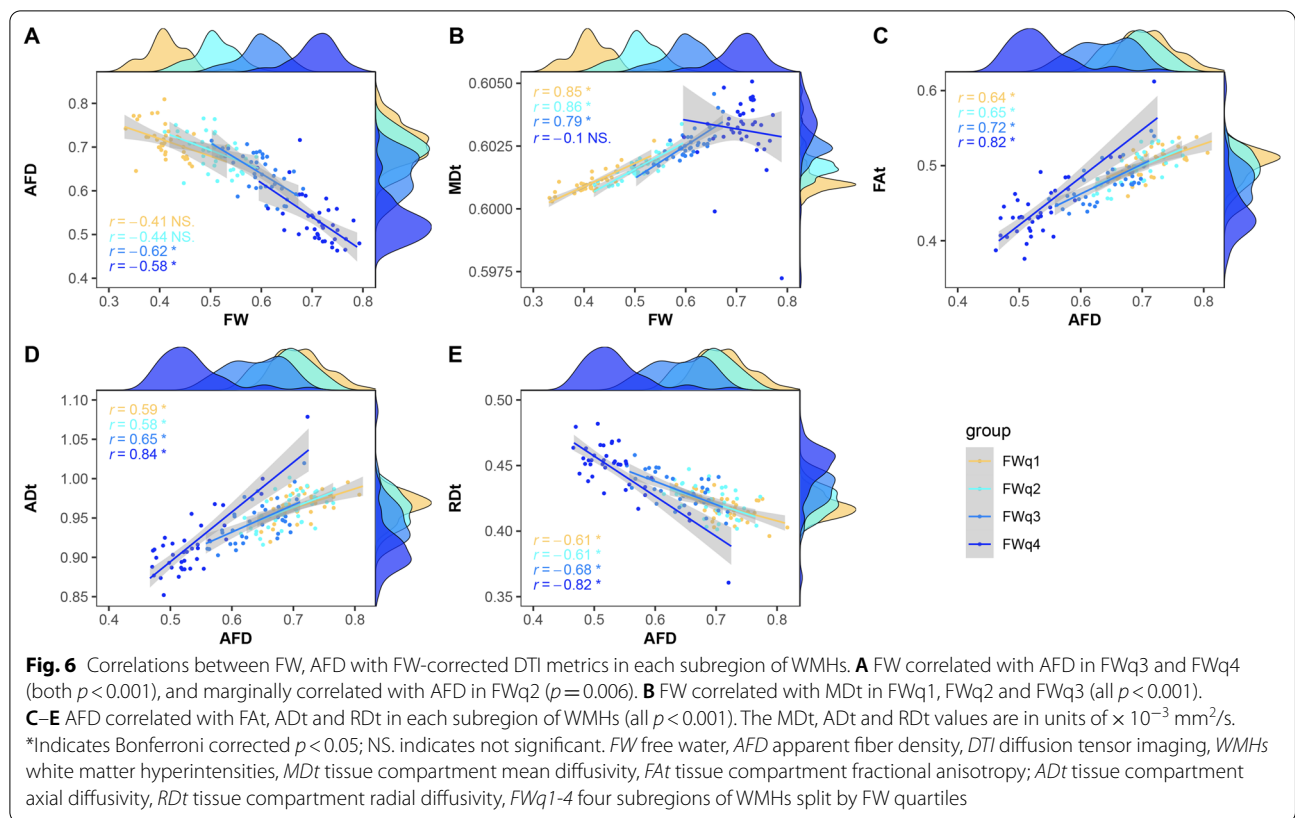


Table 2 The relationships between free water with lacunes and microbleeds using logistics regression model

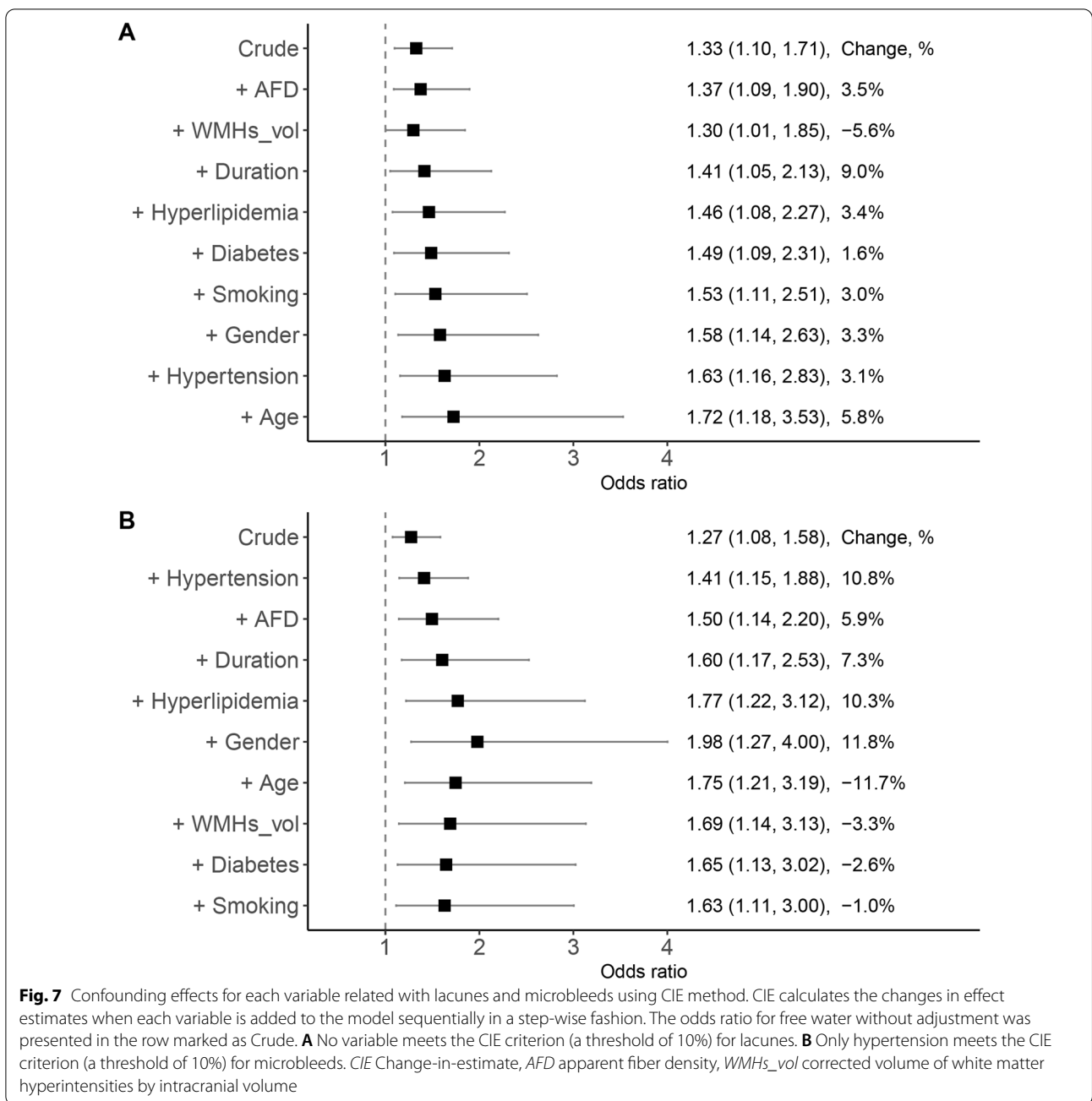
	Lacunes			Microbleeds		
	OR (95% CI)	p value	R ²	OR (95% CI)	p value	R ²
Model 1	1.33 (1.10–1.71)	0.010	0.31	1.27 (1.08–1.58)	0.010	0.27
Model 2	–	–	–	1.41 (1.15–1.88)	0.005	0.45

Model 1: crude, no adjustment; Model 2: adjusting for variables meeting the criteria of change-in-estimate approach (10% cutoff)

of perivascular lymphatic drainage, resulting in further accumulation of ISF [39]. The accumulation of ECF could cause a build-up of harmful substances such as plasma proteins from a leaky BBB [10], which are toxic to surrounding WM microstructures including myelin and axon. From a pathophysiological perspective, increased ECF possibly occurs first, followed by demyelination and axonal damage within WMHs.

The findings from our study may provide support for the above-mentioned theory. First, microstructural changes (significant correlations between FW and AFD, significant decrease in Fat and ADt, significant increase in MDt and RDt) only existed in WMHs subregions with high-level FW (FWq3 and FWq4), implying that WM microstructural damage starts to rise when ECF reaches above the median value of FW. Second, disease duration had a negative correlation (marginally

significant) with AFD but not with FW in FWq3 and FWq4, suggesting that fiber disruption occurred at relatively late disease stages. Besides, in a recent study in a large cohort of older people of similar age, MD showed the best differentiation of WMHs from NAWM, suggesting that altered water mobility in the interstitial space may be an early feature of WM pathology [40]. Due to the cross-sectional nature of the current study, we could not rule out the possibility that WM microstructural degeneration results in the accumulation of ECF. However, if microstructural degeneration occurred before the event of ECF in WM, the atrophy of WM should be observed, like Wallerian degeneration in ischemic stroke [41]. Conversely, a neuroimaging study showed that patients with CADASIL had larger WM volume than controls [42], whereas WM atrophy was rarely reported in CADASIL.



Our findings of microstructural changes (decreased AFD, FAT, ADt and increased MDt, RDt) in WMHs were consistent with previous pathological findings [43, 44]. Combined with findings of ECF distribution, microstructural damage in periventricular WMHs is more severe than that in deep WMHs.

The diffusion alterations in FAT and MDt have been described in a recent CADASIL study [8]. To better characterize the microstructural damage related with axonal degeneration and demyelination, we used additional

FW-corrected DTI metrics including ADt and RDt. Interestingly, ADt showed an opposite change in WMHs in contrast to AD, whereas other metrics showed the same direction in changes as the conventional DTI metrics. AD may increase with increased extracellular water content and reduced density of WM fibers, which allows faster water molecule movement parallel to axons [45]. This explanation is supported by our findings of increased FW and decreased AFD. The decreased ADt with increased AD has also been reported in white

matter regions heavily affected by age [46]. Although our observation of decreased ADt and increased RDt in WMHs possibly respectively represent the pathological features of axonal degeneration and demyelination [47], interpretation of them remains to be challenged by other pathological changes in WMHs like gliosis, neuroinflammation and vascular alterations.

Apart from widespread WMHs, other imaging markers including lacunes and microbleeds appearing later on brain MRI, are also related with cognitive impairments in patients with CADASIL [48, 49]. We further found that increased ECF in WMHs was independently related to both lacunes and microbleeds, which was similar to our findings from sporadic CSVD [50]. As previously mentioned, the vessel wall structure is already weak due to VSMCs degeneration in CADASIL. On this basis, the increased ECF could further aggravate the weakness of the vessel wall with compromised autoregulation of cerebral blood flow, thus resulting in insufficient perfusion and vascular rupture. Therefore, WMHs, lacunes and microbleeds may share a common pathogenesis. It should be noted that lacunes and microbleeds can in turn contribute to the increased ECF. ISF clearance in the brain is driven by arterial blood flow, while decreased perfusion caused by lacunes and microbleeds can reduce the efficiency of solute clearance by this pathway [51, 52].

Several limitations should be considered. First, this is a cross-section study and thus, the relationships between diffusion metrics (e.g., FW and AFD) should be interpreted logically and cautiously. Future follow-up studies can be conducted to prove the effects of ECF on microstructural changes in WM. Second, analysis of PVS could offer complementary evidence about the impaired drainage of ECF in the brain, such as in the anterior temporal lobe. Unfortunately, due to lack of T2-weighted images, we did not perform the analysis of PVS. Third, there is currently limited histopathological evidence to specifically validate diffusion MRI metrics. Although measuring water distribution in postmortem tissue is challenging, future studies using novel methods to make direct comparisons between new diffusion metrics and pathology will be significant to improve the specificity of diffusion markers in CADASIL. Last, the sample size is relatively small. Nevertheless, the effect size in MANOVA test reaches medium to high, indicating the reliability of our findings.

Conclusions

In summary, we demonstrated in CADASIL that increased ECF was associated with WM degeneration and the occurrence of lacunes and microbleeds, providing important new insights into the role of ECF in

CADASIL pathology. Improving ECF clearance might become a therapeutic strategy in future.

Abbreviations

AD: Axial diffusivity; ADt: Tissue compartment AD; AFD: Apparent fiber density; ANTs: Advanced Normalization Tools; BBB: Blood-brain barrier; CADASIL: Cerebral autosomal-dominant arteriopathy with subcortical infarcts and leukoencephalopathy; CSD: Constrained spherical deconvolution; CSF: Cerebrospinal fluid; CSVD: Cerebral small vessel disease; DTI: Diffusion tensor imaging; ECF: Extracellular fluid; EPI: Echo-planar imaging; FA: Fractional anisotropy; FAT: Tissue compartment FA; FLAIR: Fluid-attenuated inversion recovery; FODs: Fiber orientation distributions; FSL: FMRIB Software Library; FW: Free water; GM: Gray matter; GOM: Granular osmiophilic material; ICV: Intracranial volumes; ISF: Interstitial fluid; LPM: Lesion probability map; MANOVA: One-way multivariate analysis of variance; MD: Mean diffusivity; MDt: Tissue compartment MD; NAWM: Normal appearing white matter; OR: Odds ratio; PVS: Perivascular spaces; RD: Radial diffusivity; RDt: Tissue compartment RD; SS3T-CSD: Single-shell 3-tissue CSD; WM: White matter; WMHs: White matter hyperintensities; VSMCs: Vascular smooth muscle cells.

Supplementary Information

The online version contains supplementary material available at <https://doi.org/10.1186/s12987-021-00264-1>.

Additional file 1. Additional methods, tables and figure.

Acknowledgements

Not applicable.

Authors' contributions

XFY collected, analyzed and interpreted all the data and drafted the manuscript. XZY recruited the subjects, assisted with the design of the study, interpreted the data and revised the manuscript. HH, SYW and YJ contributed to the collection and analysis of data. FZ and OP provided the diffusion MRI post-processing method and revised the manuscript. RTZ, LLY and ML assisted with the subjects recruitment and data interpretation. MMZ and PYH assisted with the design of the study, the set-up of subject scan protocol, supervised the work and revised the manuscript. All authors read and approved the final manuscript.

Funding

This study was supported by 13th Five-year Plan for National Key Research and Development Program of China (No. 2016YFC1306600), National Natural Science Foundation of China (No. 81901706, No. 81901319 & No. 81771820), Natural Science Foundation of Zhejiang Province (No. LSZ19H180001 & No. LQ20H180015), China Postdoctoral Science Foundation (No. 2019M662083) and Zhejiang province Postdoctoral Science Foundation.

Availability of data and materials

The datasets generated and/or analysed during the current study are not publicly available due to ongoing analysis for future publication, but are available from the corresponding author on reasonable request.

Declarations

Ethics approval and consent to participate

The study was approved by the Medical Ethics Committee of the Second Affiliated Hospital, Zhejiang University School of Medicine.

Consent for publication

Written informed consent for publication was obtained from all subjects.

Competing interests

The authors disclose no conflicts of interest.

Author details

¹Department of Radiology, The 2nd Affiliated Hospital, Zhejiang University School of Medicine, No.88 Jiefang Road, Shangcheng District, Hangzhou 310009, China. ²Department of Neurology, The 2nd Affiliated Hospital, Zhejiang University School of Medicine, Hangzhou, China. ³Department of Radiology, Brigham and Women's Hospital, Harvard Medical School, Boston, MA, USA. ⁴Department of Psychiatry, Brigham and Women's Hospital, Harvard Medical School, Boston, MA, USA. ⁵Department of Psychiatry, The 2nd Affiliated Hospital, Zhejiang University School of Medicine, Hangzhou, China.

Received: 13 April 2021 Accepted: 19 June 2021

Published online: 30 June 2021

References

- Debette S, Markus H. The clinical importance of white matter hyperintensities on brain magnetic resonance imaging: systematic review and meta-analysis. *BMJ*. 2010. <https://doi.org/10.1136/bmj.c3666>.
- Prins ND, Scheltens P. White matter hyperintensities, cognitive impairment and dementia: an update. *Nat Rev Neurol*. 2015;11:157–65.
- Hasan TF, Barrett KM, Brott TG, Badi MK, Lesser ER, Hodge DO, et al. Severity of white matter hyperintensities and effects on all-cause mortality in the Mayo Clinic Florida Familial Cerebrovascular Diseases Registry. *Mayo Clin Proc*. 2019;94:408–16.
- Di Donato I, Bianchi S, De Stefano N, Dichgans M, Dotti MT, Duering M, et al. Cerebral autosomal dominant arteriopathy with subcortical infarcts and leukoencephalopathy (CADASIL) as a model of small vessel disease: update on clinical, diagnostic, and management aspects. *BMC Med*. 2017;15:1–12.
- Joutel A, Corpechot C, Ducros A, Vahedi K, Chabriat H, Mouton P, et al. Notch3 mutations in CADASIL, a hereditary adult-onset condition causing stroke and dementia. *Nature*. 1996;383:707–10.
- Singhal S, Bevan S, Barrick T, Rich P, Markus HS. The influence of genetic and cardiovascular risk factors on the CADASIL phenotype. *Brain*. 2004;127:2031–8.
- Yamamoto Y, Ihara M, Tham C, Low RW, Slade JY, Moss T, et al. Neuro-pathological correlates of temporal pole white matter hyperintensities in CADASIL. *Stroke*. 2009;40:2004–11.
- Duering M, Finsterwalder S, Baykara E, Tuladhar AM, Gesierich B, Konieczny MJ, et al. Free water determines diffusion alterations and clinical status in cerebral small vessel disease. *Alzheimers Dement*. 2018;14:764–74.
- De Guio F, Vignaud A, Chabriat H, Jouvent E. Different types of white matter hyperintensities in CADASIL: insights from 7-Tesla MRI. *J Cereb Blood Flow Metab*. 2018;38:1654–63.
- Tikka S, Baumann M, Siitonen M, Pasanen P, Pöyhönen M, Myllykangas L, et al. CADASIL and CARASIL. *Brain Pathol*. 2014;24:525–44.
- Weller RO, Hawkes CA, Kalaria RN, Werring DJ, Carare RO. White matter changes in dementia: role of impaired drainage of interstitial fluid. *Brain Pathol*. 2015;25:63–78.
- Jones DK, Knösche TR, Turner R. White matter integrity, fiber count, and other fallacies: the do's and don'ts of diffusion MRI. *Neuroimage*. 2013;73:239–54.
- Pasternak O, Sochen N, Gur Y, Intrator N, Assaf Y. Free water elimination and mapping from diffusion MRI. *Magn Reson Med*. 2009;62:717–30.
- Raffelt D, Tournier J-D, Rose S, Ridgway GR, Henderson R, Crozier S, et al. Apparent fibre density: a novel measure for the analysis of diffusion-weighted magnetic resonance images. *Neuroimage*. 2012;59:3976–94.
- Yin X, Zhou Y, Yan S, Lou M. Effects of cerebral blood flow and white matter integrity on cognition in CADASIL patients. *Front Psych*. 2019;9:741.
- Tang Y, Pasternak O, Kubicki M, Rathi Y, Zhang T, Wang J, et al. Altered cellular white matter but not extracellular free water on diffusion MRI in individuals at clinical high risk for psychosis. *Am J Psychiatry*. 2019;176:820–8.
- Dhollander T, Mito R, Raffelt D, Connelly A. Improved white matter response function estimation for 3-tissue constrained spherical deconvolution. In: 27th International Society of Magnetic Resonance in Medicine, Montréal, Québec, Canada. 2019. p. 555.
- Mito R, Dhollander T, Xia Y, Raffelt D, Salvado O, Churilov L, et al. In vivo microstructural heterogeneity of white matter lesions in healthy elderly and Alzheimer's disease participants using tissue compositional analysis of diffusion MRI data. *Neuroimage Clin*. 2020;28:102479.
- Raffelt D, Dhollander T, Tournier J-D, Tabbara R, Smith RE, Pierre E, et al. Bias field correction and intensity normalisation for quantitative analysis of apparent fibre density. In: 25th International Society of Magnetic Resonance in Medicine, Honolulu, Hawaii, United States. 2017. p. 541.
- Schmidt P. Bayesian inference for structured additive regression models for large-scale problems with applications to medical imaging. PhD thesis. Ludwig-Maximilians-Universität München; 2017. <http://nbn-resolving.org/urn:nbn:de:bvb:19-203731>.
- Egger C, Opfer R, Wang C, Kepp T, Sormani MP, Spies L, et al. MRI FLAIR lesion segmentation in multiple sclerosis: does automated segmentation hold up with manual annotation? *NeuroImage Clin*. 2017;13:264–70.
- Di Perri C, Battaglini M, Stromillo ML, Bartolozzi ML, Guidi L, Federico A, et al. Voxel-based assessment of differences in damage and distribution of white matter lesions between patients with primary progressive and relapsing-remitting multiple sclerosis. *Arch Neurol*. 2008;65:236–43.
- Bodini B, Battaglini M, De Stefano N, Khaleeli Z, Barkhof F, Chard D, et al. T2 lesion location really matters: a 10 year follow-up study in primary progressive multiple sclerosis. *J Neurol Neurosurg Psychiatry*. 2011;82:72–7.
- Wardlaw JM, Smith EE, Biessels GJ, Cordonnier C, Fazekas F, Frayne R, et al. Neuroimaging standards for research into small vessel disease and its contribution to ageing and neurodegeneration. *Lancet Neurol*. 2013;12:822–38.
- Wang Z. Two postestimation commands for assessing confounding effects in epidemiological studies. *Stata Journal*. 2007;7:183–96.
- Witte J, Didelez V. Covariate selection strategies for causal inference: classification and comparison. *Biom J*. 2019;61:1270–89.
- Fernando MS, Simpson JE, Matthews F, Brayne C, Lewis CE, Barber R, et al. White matter lesions in an unselected cohort of the elderly: molecular pathology suggests origin from chronic hypoperfusion injury. *Stroke*. 2006;37:1391–8.
- Ghosh M, Balbi M, Hellal F, Dichgans M, Lindauer U, Plesnila N. Pericytes are involved in the pathogenesis of cerebral autosomal dominant arteriopathy with subcortical infarcts and leukoencephalopathy. *Ann Neurol*. 2015;78:887–900.
- Moody DM, Brown WR, Challa VR, Anderson RL. Periventricular venous collagenosis: association with leukoaraiosis. *Radiology*. 1995;194:469–76.
- Maillard P, Mitchell GF, Himali JJ, Beiser A, Fletcher E, Tsao CW, et al. Aortic stiffness, increased white matter free water, and altered microstructural integrity: a continuum of injury. *Stroke*. 2017;48:1567–73.
- Keith J, Gao F-q, Noor R, Kiss A, Balasubramaniam G, Au K, et al. Collagenosis of the deep medullary veins: an underrecognized pathologic correlate of white matter hyperintensities and periventricular infarction? *J Neuropathol Exp Neurol*. 2017;76:299–312.
- Pettersen JA, Keith J, Gao F, Spence JD, Black SE. CADASIL accelerated by acute hypotension: arterial and venous contribution to leukoaraiosis. *Neurology*. 2017;88:1077–80.
- Zhang R, Huang P, Jiaerken Y, Wang S, Hong H, Luo X, et al. Venous disruption affects white matter integrity through increased interstitial fluid in cerebral small vessel disease. *J Cereb Blood Flow Metab*. 2021;41:157–65.
- Wardlaw JM, Benveniste H, Nedergaard M, Zlokovic BV, Mestre H, Lee H, et al. Perivascular spaces in the brain: anatomy, physiology and pathology. *Nat Rev Neurol*. 2020;16:137–53.
- Huang P, Zhang R, Jiaerken Y, Wang S, Yu W, Hong H, et al. Deep white matter hyperintensity is associated with the dilation of perivascular space. *J Cereb Blood Flow Metab*. 2021. <https://doi.org/10.1177/0271678X211002279>.
- Griffanti L, Jenkinson M, Suri S, Zsoldos E, Mahmood A, Filippini N, et al. Classification and characterization of periventricular and deep white matter hyperintensities on MRI: a study in older adults. *Neuroimage*. 2018;170:174–81.
- Engelhardt B, Carare RO, Bechmann I, Flügel A, Laman JD, Weller RO. Vascular, glial, and lymphatic immune gateways of the central nervous system. *Acta Neuropathol*. 2016;132:317–38.
- Yamamoto Y, Craggs LJ, Watanabe A, Booth T, Attems J, Low RW, et al. Brain microvascular accumulation and distribution of the NOTCH3 ectodomain and granular osmiophilic material in CADASIL. *J Neuropathol Exp Neurol*. 2013;72:416–31.
- Carare R, Hawkes C, Jeffrey M, Kalaria R, Weller R. Cerebral amyloid angiopathy, prion angiopathy, CADASIL and the spectrum of protein elimination failure angiopathies (PEFA) in neurodegenerative disease with a focus on therapy. *Neuropathol Appl Neurobiol*. 2013;39:593–611.

40. Maniega SM, Hernández MCV, Clayden JD, Royle NA, Murray C, Morris Z, et al. White matter hyperintensities and normal-appearing white matter integrity in the aging brain. *Neurobiol Aging*. 2015;36:909–18.
41. Kuhn M, Mikulis D, Ayoub D, Kosofsky B, Davis K, Taveras J. Wallerian degeneration after cerebral infarction: evaluation with sequential MR imaging. *Radiology*. 1989;172:179–82.
42. De Guio F, Mangin J-F, Duering M, Ropele S, Chabriat H, Jouvent E. White matter edema at the early stage of cerebral autosomal-dominant arteriopathy with subcortical infarcts and leukoencephalopathy. *Stroke*. 2015;46:258–61.
43. Gouw AA, Seewann A, Van Der Flier WM, Barkhof F, Rozemuller AM, Scheltens P, et al. Heterogeneity of small vessel disease: a systematic review of MRI and histopathology correlations. *J Neurol Neurosurg Psychiatry*. 2011;82:126–35.
44. Murray ME, Vemuri P, Preboske GM, Murphy MC, Schweitzer KJ, Parisi JE, et al. A quantitative postmortem MRI design sensitive to white matter hyperintensity differences and their relationship with underlying pathology. *J Neuropathol Exp Neurol*. 2012;71:1113–22.
45. Della Nave R, Ginestroni A, Diciotti S, Salvatore E, Soricelli A, Mascalchi M. Axial diffusivity is increased in the degenerating superior cerebellar peduncles of Friedreich's ataxia. *Neuroradiology*. 2011;53:367–72.
46. Chad JA, Pasternak O, Salat DH, Chen JJ. Re-examining age-related differences in white matter microstructure with free-water corrected diffusion tensor imaging. *Neurobiol Aging*. 2018;71:161–70.
47. Sun SW, Liang HF, Trinkaus K, Cross AH, Armstrong RC, Song SK. Noninvasive detection of cuprizone induced axonal damage and demyelination in the mouse corpus callosum. *Magn Reson Med*. 2006;55:302–8.
48. Jouvent E, Duering M, Chabriat H. Cerebral autosomal dominant arteriopathy with subcortical infarcts and leukoencephalopathy: lessons from neuroimaging. *Stroke*. 2020;51:21–8.
49. Chung CP, Chen JW, Chang FC, Li WC, Lee YC, Chen LF, et al. Cerebral microbleed burdens in specific brain regions are associated with disease severity of cerebral autosomal dominant arteriopathy with subcortical infarcts and leukoencephalopathy. *J Am Heart Assoc*. 2020;9:e016233.
50. Huang P, Zhang R, Jiaerken Y, Wang S, Hong H, Yu W, et al. White matter free water is a composite marker of cerebral small vessel degeneration. *Trans Stroke Res*. 2021. <https://doi.org/10.1007/s12975-021-00899-0>.
51. Arbel-Ornath M, Hudry E, Eikermann-Haerter K, Hou S, Gregory JL, Zhao L, et al. Interstitial fluid drainage is impaired in ischemic stroke and Alzheimer's disease mouse models. *Acta Neuropathol*. 2013;126:353–64.
52. Gregg NM, Kim AE, Guroi ME, Lopez OL, Aizenstein HJ, Price JC, et al. Incidental cerebral microbleeds and cerebral blood flow in elderly individuals. *JAMA Neurol*. 2015;72:1021–8.

Publisher's Note

Springer Nature remains neutral with regard to jurisdictional claims in published maps and institutional affiliations.

Ready to submit your research? Choose BMC and benefit from:

- fast, convenient online submission
- thorough peer review by experienced researchers in your field
- rapid publication on acceptance
- support for research data, including large and complex data types
- gold Open Access which fosters wider collaboration and increased citations
- maximum visibility for your research: over 100M website views per year

At BMC, research is always in progress.

Learn more biomedcentral.com/submissions

